Monthly Notices of the ROYAL ASTRONOMICAL SOCIETY

MNRAS **511,** 5927–5935 (2022) https://doi.org/10.1093/mnras/stac406
Advance Access publication 2022 February 17

The effects of self-interacting dark matter on the stripping of galaxies that fall into clusters

Ellen L. Sirks ,★ Kyle A. Oman , Andrew Robertson , Richard Massey and Carlos Frenk
Institute for Computational Cosmology, Department of Physics, Durham University, South Road, Durham DH1 3LE, UK

Accepted 2022 February 7. Received 2022 January 17; in original form 2021 September 7

ABSTRACT

We use the Cluster-EAGLE (C-EAGLE) hydrodynamical simulations to investigate the effects of self-interacting dark matter (SIDM) on galaxies as they fall into clusters. We find that SIDM galaxies follow similar orbits to their cold dark matter (CDM) counterparts, but end up with ∼25 per cent less mass by the present day. One in three SIDM galaxies is entirely disrupted, compared to one in five CDM galaxies. However, the excess stripping will be harder to observe than suggested by previous DM-only simulations because the most stripped galaxies form cores and also lose stars: The most discriminating objects become unobservable. The best test will be to measure the stellar-to-halo mass relation (SHMR) for galaxies with stellar mass 10^{10}–10^{11} $M_\odot$. This is 8 times higher in a cluster than in the field for a CDM universe, but 13 times higher for an SIDM universe. Given intrinsic scatter in the SHMR, these models could be distinguished with noise-free galaxy–galaxy strong lensing of ∼32 cluster galaxies.

Key words: galaxies: clusters: general – galaxies: haloes – dark matter – cosmology: theory.

1 INTRODUCTION

As galaxies fall into clusters, they are transformed, morphologically and spectroscopically. Their gas content, hitting the intracluster gas, is shocked. Turbulence causes a sudden, final burst of star formation – before ram pressure and gravitational tides strip it away, quenching star formation thereafter (e.g. McCarthy et al. 2008; van den Bosch et al. 2008; Oman et al. 2021). The galaxies' dark matter (DM) is also eventually stripped by tidal gravity and gradually becomes incorporated into the (now slightly larger) cluster. This is the key mechanism for the growth of structure in the Universe; yet, the timescale for DM stripping and virialization remains poorly understood.

In the standard Λ cold dark matter (ΛCDM) model of cosmology, DM particles interact with each other only through gravity. The model successfully explains all observables at large scales, such as the galaxy clustering signal (for a review, see Frenk & White 2012) and the cosmic microwave background anisotropy (e.g. Planck Collaboration et al. 2016). However, there is no a priori reason why DM particles should not interact with each other (Burkert 2000; Spergel & Steinhardt 2000), and weak self-interactions are a natural consequence of some particle physics theories for the origin of DM (for a review, see e.g. Tulin & Yu 2018). With a mean free path ranging from 1 kpc to 1 Mpc, DM self-interactions would preserve the large-scale success of ΛCDM, and could resolve tensions between the results of DM-only simulations and observations of dwarf and low-mass galaxies (for a review, see Bullock & Boylan-Kolchin 2017).

Massive galaxy clusters are a promising environment to search for DM–DM interactions, because the interaction rate would be proportional to the local DM density and to the local velocity dispersion of DM particles (for a review, see Massey, Kitching & Richard 2010). Observations have placed several limits on the strength of the self-interacting dark matter (SIDM) cross-section per unit mass (σ/m) at the typical velocities encountered in clusters, including $\sigma/m \lesssim 1\,\mathrm{cm^2\,g^{-1}}$ (Peter et al. 2013, from cluster halo shapes), $\sigma/m < 1\,\mathrm{cm^2\,g^{-1}}$ (Rocha et al. 2013, from cluster core sizes), $\sigma/m < 0.1\,\mathrm{cm^2\,g^{-1}}$ (Meneghetti et al. 2001, from strong lensing arc statistics, but see also Vega-Ferrero et al. 2021), and $\sigma/m < 0.47\,\mathrm{cm^2\,g^{-1}}$ (Harvey et al. 2015, from DM-galaxy offsets in merging clusters, but see also Wittman, Golovich & Dawson 2018). Merging clusters are sufficiently rare that interpretation of them tends to be limited by uncertainty in their orientation with respect to the line of sight (Clowe et al. 2006; Bradač et al. 2008; Dawson et al. 2012). However, the promising prospects revealed by Robertson, Massey & Eke (2017a)'s detailed study of high-velocity DM collisions motivate a search for more ubiquitous examples of objects falling into clusters.

Whenever a galaxy falls into an SIDM cluster, interactions between its DM particles and those in the cluster could scatter DM out of the galaxy. This 'evaporation' acts in addition to tidal stripping and accelerates overall mass-loss. The orbits of infalling galaxies might also be changed. Galaxies spiral towards the centre of a cluster due to dynamical friction, which has strength proportional to the galaxy's mass (Binney & Tremaine 2008, chapter 8). If galaxies lose additional mass, they might sink less far or more slowly into the cluster. On the other hand, drag due to the DM self-interactions (which may be positive or negative; Robertson et al. 2017a) could increase the rate of decay or inhibit the formation of trailing density wakes in the first place (Di Cintio et al. 2017).

★ E-mail: ellen.l.sirks@durham.ac.uk

Table 1. Properties of the CDM and SIDM versions of the two C-EAGLE clusters at redshift $z = 0$.

Simulation	DM type	$M_{200}/\mathrm{M}_\odot$	R_{200}/Mpc	$N_{\rm tot}$
CE-05	CDM	1.38×10^{14}	1.09	1442
	SIDM	1.36×10^{14}	1.09	1183
CE-12	CDM	3.96×10^{14}	1.55	3893
	SIDM	3.91×10^{14}	1.54	2938

The mass M_{200} is that enclosed within the sphere of physical radius R_{200} whose mean density is 200 times the critical density of the Universe. Cluster member galaxies are the $N_{\rm gal}$ subhaloes in the FoF group of the cluster that are within $2R_{200}$ of the cluster centre and contain one or more star particles.

The aims of this paper are to study the differences in DM mass-loss and orbital dynamics of cluster galaxies, using hydrodynamical simulations with CDM and SIDM physics – and to investigate whether the differences would be observable. The only previous study of such effects used DM-only simulations (Bhattacharyya et al. 2021).

This paper is organized as follows: in Section 2, we present the simulation suite used in this work; in Section 3, we study the effects of self-interactions by matching galaxies between our CDM and SIDM simulations; and in Section 4, we investigate the effects on observables using the population of galaxies at $z = 0$. Finally, we discuss our results and present our conclusions in Section 5.

2 DATA

2.1 The EAGLE and Cluster-EAGLE simulations

We use the 50 Mpc EAGLE cosmological simulation (Schaye et al. 2015) and the Cluster-EAGLE (C-EAGLE) zoom cosmological simulations of smaller volumes centred on $\gtrsim 10^{14}\,\mathrm{M}_\odot$ galaxy clusters (Bahé et al. 2017). Both were run with a modified version of the GADGET-3 code that includes radiative cooling, star formation, chemical evolution, and stellar and active galactic nucleus (AGN) feedback (with the 'AGNdT9' feedback model; Crain et al. 2015; Schaye et al. 2015). The DM particle mass is $9.7 \times 10^6\,\mathrm{M}_\odot$, the initial gas particle mass is $1.8 \times 10^6\,\mathrm{M}_\odot$, and the gravitational softening length was set to 2.66 comoving kpc before $z = 2.8$, and then kept fixed at 0.7 physical kpc at $z < 2.8$. The simulations assume cosmological parameters from Planck Collaboration et al. (2014).

The EAGLE volume and two of the C-EAGLE clusters, CE-05 and CE-12, have been re-simulated from identical initial conditions in a ΛSIDM universe (see Table 1 and Robertson et al. 2018 for more details). These two particular C-EAGLE clusters are 'relaxed', based on their gas properties at $z = 0.1$ (Barnes et al. 2017). Since CE-12 is slightly more massive, and has more member galaxies, we shall quote the higher signal-to-noise statistics from that cluster whenever we study the differences between CDM and SIDM at $z = 0$. However, no data are available for that cluster at higher redshift, so we shall use CE-05 whenever we trace the evolution of DM through time. Note that the central galaxy in CE-05 happened to form early, and the central density cusp has been retained in both CDM and SIDM. The central galaxy of CE-12 formed later, and SIDM interactions created a ∼100 kpc constant-density core by $z = 0$. In the inner ∼100 kpc, a few satellites enter, and if they do, they stay for a short time, and so we expect the effect from the constant-density core in CE-12 to be negligible compared to the cluster being more massive.

Our implementation of SIDM assumes an isotropic, velocity-independent interaction cross-section, $\sigma/m = 1\,\mathrm{cm}^2\,\mathrm{g}^{-1}$. This is around the upper limit of values compatible with current measurements, and therefore maximizes the observable consequences. During each simulation time-step, Δt, DM particles scatter elastically off neighbours within radius $h_{\rm SI} = 2.66$ kpc (comoving) with probability

$$P_{\rm scat} = \frac{(\sigma/m)\, m_{\rm DM}\, v\, \Delta t}{\frac{4\pi}{3} h_{\rm SI}^3}\,, \tag{1}$$

where v is the particles' relative velocity and $m_{\rm DM}$ the DM particle mass (for more details, see Robertson, Massey & Eke 2017b). We log the time and particle IDs of all DM scattering events. This enables us to distinguish between: DM particles that have not scattered, those that have scattered with other DM particles from their own (sub)halo, and those that have scattered with DM particles from elsewhere in the cluster.

2.2 Finding and tracking individual galaxies

We detect groups of particles in the simulations using a FRIENDS-OF-FRIENDS (FoF; Davis et al. 1985) algorithm with linking length 0.2, and identify individual subhaloes (in all 30 simulation snapshots from $z = 14$ to 0) using the SUBFIND (Springel et al. 2001; Dolag et al. 2009) algorithm. For SUBFIND to identify a galaxy, it must have at least 20 particles. We track subhaloes between snapshots and construct their merger trees using the D-TREES algorithm (Jiang et al. 2014). This identifies each subhalo's $N_{\rm link}$ most bound particles of any species, with $N_{\rm link} = \min(100, \max(0.1 N_{\rm gal}, 10))$, where $N_{\rm gal}$ is the total number of particles in the subhalo in each snapshot. The descendant of a subhalo is the object that contains most of these $N_{\rm link}$ particles in the next snapshot. A subhalo can have multiple progenitors in the previous snapshot, but we define the main progenitor as that for which the mass summed across all earlier snapshots is the largest. The main branch of a subhalo is comprised of its main progenitors and descendants. We use the main branches of subhaloes to trace their properties through time.

We identify as 'field galaxies' all SUBFIND central haloes (rank 0 in a given FoF group) in EAGLE, which contain at least one star particle. We identify as 'cluster member galaxies' all SUBFIND subhaloes in C-EAGLE, which contain at least one star particle and are within radius $2R_{200}$. We define their time of infall as the first snapshot after they enter that radius for the first time. By keeping all galaxies within $2R_{200}$, we include those galaxies that have already passed through the cluster once (and thus have felt its effects) and have passed beyond R_{200} again, i.e. the splashback population. Additionally, by keeping galaxies within $2R_{200}$, we end up with a larger number of total and high-mass galaxies.

The mass of every galaxy is defined as the total mass, $M_{\rm tot}$, of all particles gravitationally bound to it (i.e. the mass $M_{\rm SUB}$ assigned to the subhalo by the SUBFIND algorithm). Its stellar mass, $M_\star$, is defined as the total mass of stars within twice its half-light radius. Its location is defined by the location of its constituent particle with the lowest gravitational potential energy.

2.3 The stellar-to-halo mass relation

Below, we will compare the stellar-to-halo mass relations (SHMRs) of galaxies in our SIDM and CDM models. We fit the SHMR to a population of simulated galaxies using the form of the Moster, Naab & White (2013) relation derived from abundance matching,

$$M_\star(M_{\rm tot}) = 2N M_{\rm tot} \left[\left(\frac{M_{\rm tot}}{M_1} \right)^{-\beta} + \left(\frac{M_{\rm tot}}{M_1} \right)^{\gamma} \right]^{-1}. \tag{2}$$

By numerically inverting equation (2), we also fit $M_{\rm tot}(M_\star)$, which can be measured observationally.

We use the Markov chain Monte Carlo (MCMC) sampler EMCEE (Foreman-Mackey et al. 2013) to obtain the best-fitting values and posterior probability density functions (PDFs) of the free parameters, M_1, N, β, γ, as well as the free parameter, $\sigma_{\rm M}$, the scatter in stellar mass (or in total mass for the inverse fit), which we assume to be constant. The latter enters the fit through the log-likelihood function,

$$\log\mathcal{L} = -\frac{1}{2}\sum_{i=1}^{N}\left(\frac{\log M_i - \log M_i^{\rm mod}}{\sigma_{\rm M}}\right)^2 - \frac{N}{2}\log\left(2\pi\sigma_{\rm M}^2\right), \qquad (3)$$

where the summation is over the total number of galaxies, N; M_i is the stellar/total mass of galaxy i, and $M_i^{\rm mod}$ is the modelled stellar/total mass of galaxy i, for a given set of parameters. When fitting the SHMR, we truncate fits at the mass where each galaxy includes at least 10 star particles.

2.4 Matching galaxies between simulations

We match galaxies between the CDM and SIDM simulations, so their evolution can be individually compared. In the snapshot after each galaxy crosses $2R_{200}$, we identify its counterpart in the other simulation as that which contains the highest fraction, $f_{\rm match}$, of shared particle IDs

$$f_{\rm match} = \frac{N_{\rm shared}^2}{N_{\rm CDM,tot}N_{\rm SIDM,tot}}, \qquad (4)$$

where $N_{\rm shared}$ is the number of DM particles the CDM galaxy and a possible matching SIDM galaxy have in common, $N_{\rm CDM,tot}$ the total number of DM particles in the CDM galaxy, and $N_{\rm SIDM,tot}$ the total number of DM particles in the SIDM galaxy. To complete an association, we require a bijective match: i.e. the CDM galaxy points to an SIDM galaxy that points back to it. The paired CDM and SIDM galaxies inevitably have slightly different infall masses and infall times. When we bin by these, we use the CDM values. This is an arbitrary choice, but none of our results change qualitatively when using either SIDM or common bins (with logarithmic bins of 1 dex in mass, only 10 per cent of galaxies are binned differently).

When analysing matched galaxies, we ignore any cluster galaxies that were unmatched to cluster galaxies, and any field galaxies that were unmatched to a central galaxy. In cluster CE-12, 96 out of 889 CDM cluster galaxies were matched to the central galaxy of the SIDM cluster. For the field galaxies, 383 out of 9126 CDM galaxies were matched to a satellite galaxy in the SIDM simulation.

3 EVOLUTION OF DM SINCE INFALL

In this section, we examine the effect of self-interactions on the DM mass of galaxies after they fall into the clusters, by directly matching galaxies between the CDM and SIDM simulations.

3.1 The behaviour of one example galaxy

To build intuition, we first track the DM halo of one galaxy in detail. We identify a typical galaxy that fell into the cluster CE-05 at $z = 1.99$ with mass $2.7 \times 10^{11}\,{\rm M}_\odot$, and track the six-dimensional (6D) phase-space coordinates (cluster-centric radius and velocity) of all its DM particles to 2 Gyr ($z = 1.15$) and 10.5 Gyr ($z = 0$) after infall. The result is illustrated in Fig. 1, which shows that self-interactions increase the mass-loss of the SIDM galaxy compared to its CDM counterpart, but the orbit is unaffected.

3.1.1 Dark matter loss

The velocity dispersion of DM within the galaxy is reflected in the 'Fingers of God' extending towards positive and negative radial velocities. Tidally stripped DM extends both forwards and backwards along the galaxy's orbit: By 2 Gyr, some particles have already passed through pericentre and are now moving back out. On a phase-space diagram, tidally stripped material moves along the same path as the galaxy it has been removed from, both in the case of CDM and SIDM. However, the evaporated material should occupy a region distinct from the galaxy and tidally stripped material.

We separate the SIDM into particles that have scattered with DM particles in the cluster and particles that have not (Fig. 1). Note that some scattering events result in very low exchange of momentum or merely swap particle trajectories, so the scattered particles include some that have barely been perturbed. However, we find many DM particles that do not follow the tidally stripped material and therefore must be evaporated DM. After 2 Gyr, the CDM galaxy has lost roughly 54 per cent of its DM mass since infall, whereas the SIDM galaxy has lost approximately 76 per cent of its DM mass. By $z = 0$, these fractions have increased to 91 per cent and 99 per cent. Evaporation has increased the mass-loss in the SIDM galaxy with respect to its CDM counterpart.

We find a much greater SIDM mass-loss from galaxies in clusters, than Dooley et al. (2016, fig. 9) found for dwarf galaxies in the Milky Way (with the same SIDM cross-section, only a few per cent more than CDM, 10 Gyr after accretion). This striking difference is probably due to the much greater DM density and scattering rate in a cluster, but occurs despite the deeper potential wells.

3.1.2 Orbital evolution

After 2 Gyr, the CDM galaxy has moved to a 3D cluster-centric radius of ∼0.4 physical Mpc (pMpc), with a mean radial velocity centred on about $-500\,{\rm km\,s^{-1}}$, i.e. the galaxy is moving towards the centre of potential of the cluster (green cross on the top row of Fig. 1). Its SIDM counterpart is within ∼0.1 pMpc and has a similar mean radial velocity. By $z = 0$, the CDM galaxy has moved to a radius of ∼0.2 pMpc, with a mean velocity of about $+500\,{\rm km\,s^{-1}}$. Its SIDM counterpart has a mean velocity of about $-100\,{\rm km\,s^{-1}}$, but is located at about the same radius (green cross on the bottom row of Fig. 1). Indeed, we find that there is virtually no difference between the evolution of the 3D cluster-centric radius over time of the CDM and SIDM galaxy (not shown). Self-interactions increase the mass-loss of the galaxy, but do not have a significant effect on its orbit.

3.2 The behaviour of a population of galaxies

The galaxy used to produce Fig. 1 is just one example of the many member galaxies of cluster CE-05. In this section, we investigate the effect of self-interactions on the evolution of DM particles for a large sample of infalling galaxies.

3.2.1 Dark matter loss

In Fig. 2, we plot the cumulative distribution at redshifts[1] $z = 1$ and 0 of the fraction of DM lost from all CDM and SIDM galaxies

[1]To be precise, there is no simulation snapshot at exactly $z = 1$. The snapshot used here is actually at $z = 1.02$.

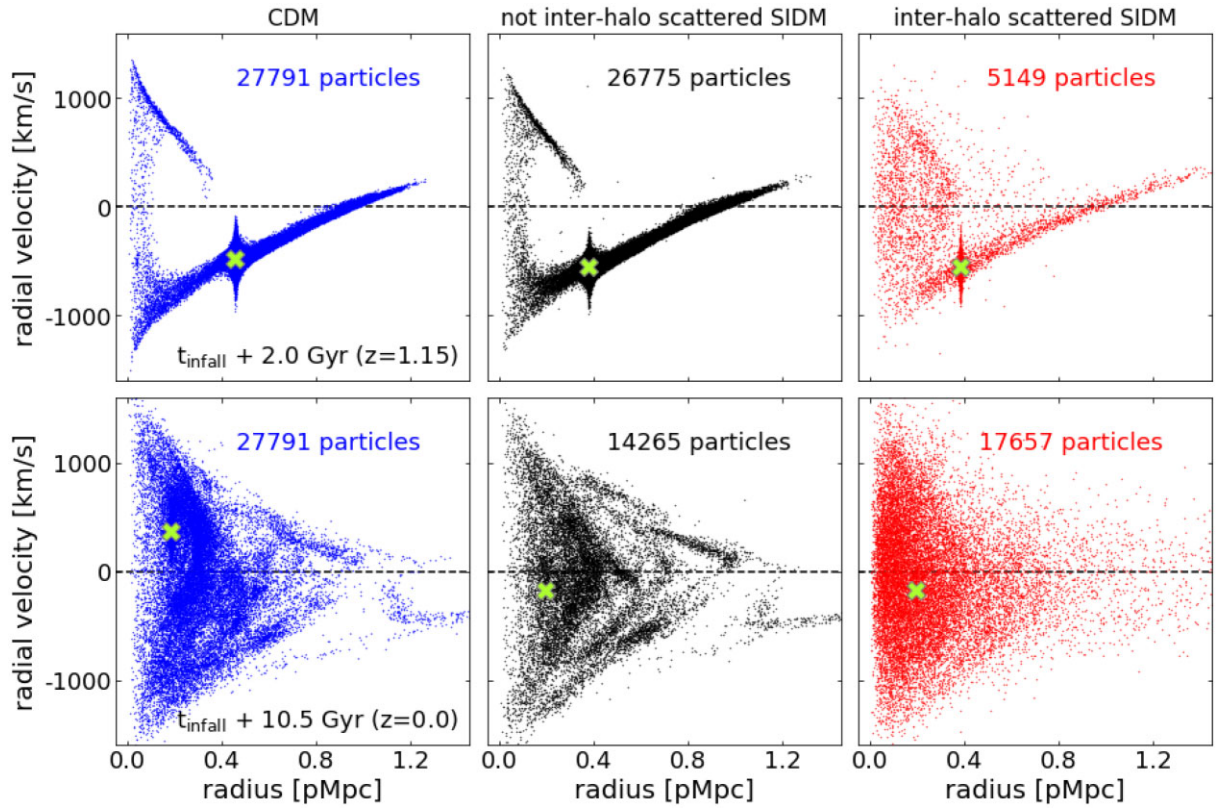

Figure 1. Cluster-centric radial velocity as a function of distance from the cluster centre for the DM in a CDM satellite of CE-05 and its SIDM counterpart, 2 Gyr (top row) and 10.5 Gyr (bottom row) after infall. Particles moving outwards from the centre of potential of the cluster have positive radial velocity. Plotted here is the DM that was in the satellite at infall. Left-hand column: the phase-space properties of the DM in the CDM galaxy. Middle column: the properties of the DM in the SIDM galaxy that has not scattered with the cluster halo DM in the time since infall. Right-hand column: same as the middle column, but for the SIDM that has scattered with the cluster halo since infall. The location of the galaxy itself is indicated by a green cross in each panel.

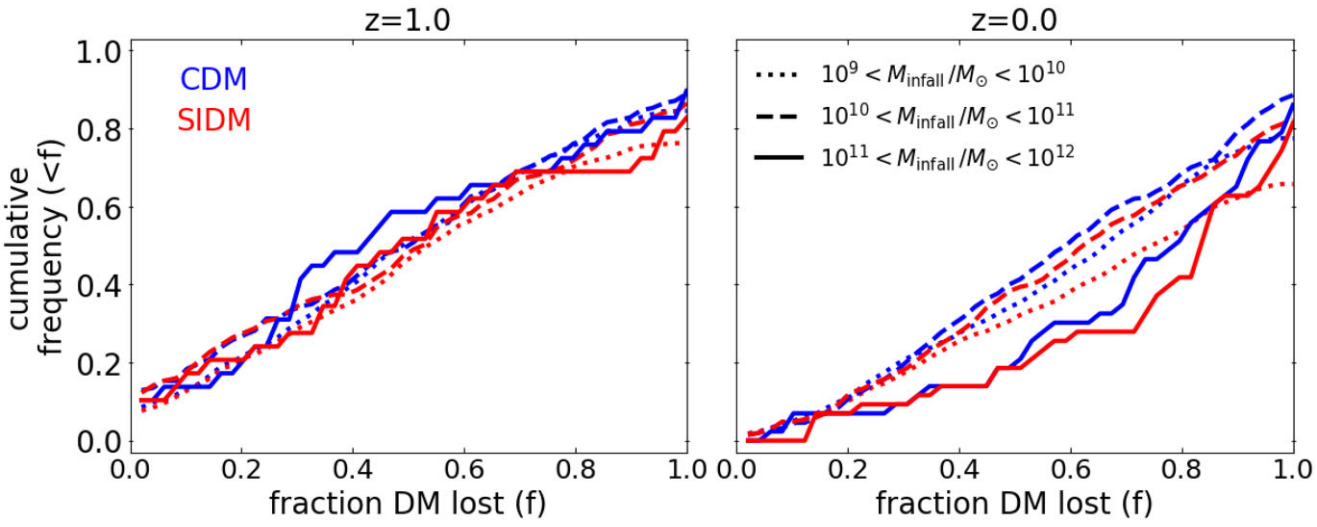

Figure 2. The cumulative frequency of galaxies with a fraction of DM lost smaller than *f*. Plotted in blue are the distributions for the CDM galaxies of CE-05, and in red their SIDM counterparts. The left-hand panel shows the results at $z = 1$, and the right-hand panel the results at $z = 0$. The different line styles represent different bins of mass at infall, as shown in the legend. A galaxy that has been completely disrupted, i.e. merged with another galaxy or with the main cluster halo, is assigned $f = 1$. The fraction of disrupted galaxies in each infall mass bin is given by 1 minus the cumulative frequency at $f = 1$, as the cumulative frequency is plotted for fractions smaller than *f*.

that were within their cluster in one or more of the 30 simulation snapshots of CE-05. We separate the galaxies into logarithmic bins of 1 dex in infall mass from 10^9 to 10^{12} $M_\odot$. When a galaxy merges with the cluster central galaxy or into the main branch of some other galaxy, we consider it to have been completely disrupted and we set the fraction of DM lost to 1.

Table 2. Fraction of disrupted cluster member galaxies of the CDM and SIDM version of CE-05, at $z = 1$ and 0 and separated into bins of 1 dex in mass at infall.

Mass range ($M_\odot$)	$z = 1$ $N_{disrupted}/N_{tot}$ CDM	$z = 1$ $N_{disrupted}/N_{tot}$ SIDM	$z = 0$ $N_{disrupted}/N_{tot}$ CDM	$z = 0$ $N_{disrupted}/N_{tot}$ SIDM
10^9–10^{10}	0.15	0.24	0.23	0.34
10^{10}–10^{11}	0.11	0.13	0.11	0.18
10^{11}–10^{12}	0.1	0.17	0.14	0.19
10^9–10^{12}	0.15	0.22	0.2	0.31

At both redshifts, we find that for a given fraction of DM lost, f, a greater fraction of the SIDM galaxies have lost a greater portion of their DM than f compared with the CDM galaxies, reflecting the increased mass-loss due to self-interactions. The biggest difference is between the low infall mass CDM and SIDM galaxies (dotted lines in Fig. 2). By $z = 0$, the mass-loss and the difference between the SIDM and CDM galaxies have increased relative to $z = 1$. We find that a larger fraction of SIDM than CDM cluster galaxies have been disrupted across all mass bins and at both redshifts; see Table 2. This is in line with our expectations, as increased mass-loss from self-interactions should lead to more disrupted cluster galaxies.

The high-mass galaxies (solid lines) have lost a greater fraction of their DM than the galaxies in the other infall mass bins (the solid lines have a different shape than the dotted and dashed lines). This is most likely a consequence of the high-mass galaxies having sunk further into the cluster, where stripping becomes more efficient. The time-scale for dynamical friction scales with the inverse of the velocity dispersion of the galaxy cubed (section 8.1.1 in Binney & Tremaine 2008), i.e. the time-scale decreases as the (infall) mass of the cluster galaxy increases.

For SUBFIND to identify a galaxy, it needs to have at least 20 particles. As a consequence, a $10^8\,M_\odot$ galaxy can only lose approximately 90 per cent of its mass before it is already considered disrupted, compared to approximately 99.9 per cent for a $10^{11}\,M_\odot$ galaxy. As a result, relatively fewer high-mass galaxies disrupt compared to low-mass galaxies, even though the high-mass galaxies tend to lose a larger fraction of their DM overall.

The cluster galaxy used to produce Fig. 1 has an infall mass of $2.7 \times 10^{11}\,M_\odot$, placing it in the high mass bin of Fig. 2. By $z = 0$, the CDM and SIDM version of this galaxy have lost approximately 91 per cent and 99 per cent of their DM mass at infall, corresponding to cumulative frequencies of approximately 0.7 and 0.8, respectively. While both have lost more of their DM than most galaxies of their (high) mass, the loss is not remarkable.

3.2.2 *Orbital evolution*

We found that the CDM galaxy and its SIDM counterpart used to produce Fig. 1 followed nearly the same orbit. To determine whether galaxy orbits in general are unaffected by self-interactions, we now consider the median evolution since the time of infall for a sample of galaxies orbiting in the cluster CE-05, in Fig. 3. We use a sample of 396 matched cluster member galaxies (see Section 2.4) from CE-05 that have $M_\star \gtrsim 10^7\,M_\odot$ at $z = 0$. Depending on their infall redshift, the galaxies have spent a different amount of time in the cluster, so a different number of galaxies contribute to each point of Fig. 3.

SIDM galaxies start losing more mass than their CDM counterparts about 2 Gyr after infall (bottom left-hand panel of Fig. 3). By 9 Gyr after infall, CDM galaxies have lost ∼75 per cent of their mass,

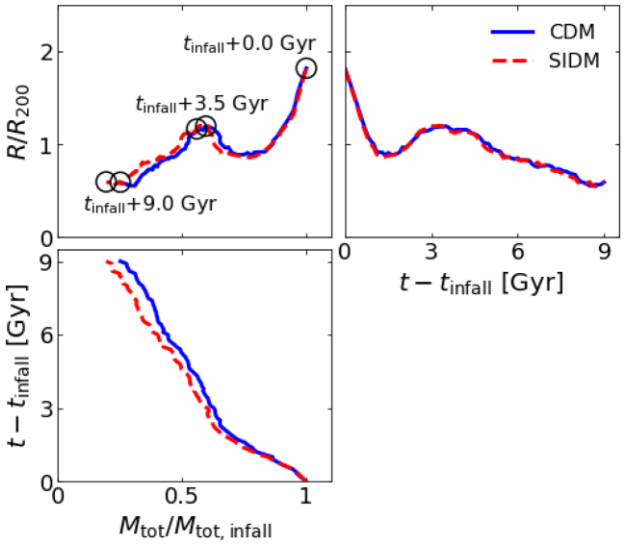

Figure 3. The median evolution since infall of cluster member galaxies with $M_\star \gtrsim 10^7\,M_\odot$ at $z = 0$, in the CDM (solid blue) and SIDM (dashed red) versions of cluster CE-05. Top left-hand panel: cluster-centric distance in units of R_{200} *versus* galaxy mass in units of galaxy mass at infall. The labels indicate the time passed since infall, and the corresponding points on both tracks are encircled. Top right-hand panel: cluster-centric distance in units of R_{200} as a function of time since infall. Bottom left-hand panel: time since infall as a function of galaxy mass in units of the galaxy mass at infall. Note that a different number of galaxies contribute to the median at every point on the plot.

while SIDM galaxies have lost ∼80 per cent. However, we find no difference between the typical orbits of CDM and SIDM galaxies that survive to $z = 0$ (top right-hand panel of Fig. 3; we shall later see very slight differences in the distribution of galaxies that do not survive).

Results are indistinguishable (but noisier) for galaxies with $M_\star \gtrsim 10^{10}\,M_\odot$. Results are also very similar in CE-12, where CDM galaxies have lost 80 per cent of their mass after 9 Gyr, and SIDM galaxies have lost 90 per cent.

4 OBSERVABLE DIFFERENCES BETWEEN CLUSTER GALAXIES IN CDM AND SIDM

We saw in Section 3 that a galaxy made of SIDM has a higher rate of DM loss than an identical galaxy made of CDM. However, observations of the real Universe do not have the luxury of matched comparisons to a control sample or null test. In this section, we investigate whether the increased rate of mass-loss has observable effects on the population of galaxies in a cluster at $z = 0$.

4.1 Stellar-to-halo mass relation

At the mass scale of individual galaxies, the SHMR of field galaxies is indistinguishable between CDM and SIDM simulations (Figs 4 and 5). This is expected because efficient gas cooling and star formation ensure that a baryon-dominated core retains a deep gravitational well (Robertson et al. 2019). Once a galaxy falls into a cluster, tidal forces preferentially remove DM, which is more diffuse than stars.

We first investigate the SHMR for matched pairs of galaxies with more than 10 star particles at $z = 0$ (Fig. 4). On average, SIDM cluster galaxies ended up with ∼0.12 dex (25 per cent) lower masses than their CDM counterparts. This effect increases to ∼0.2 dex

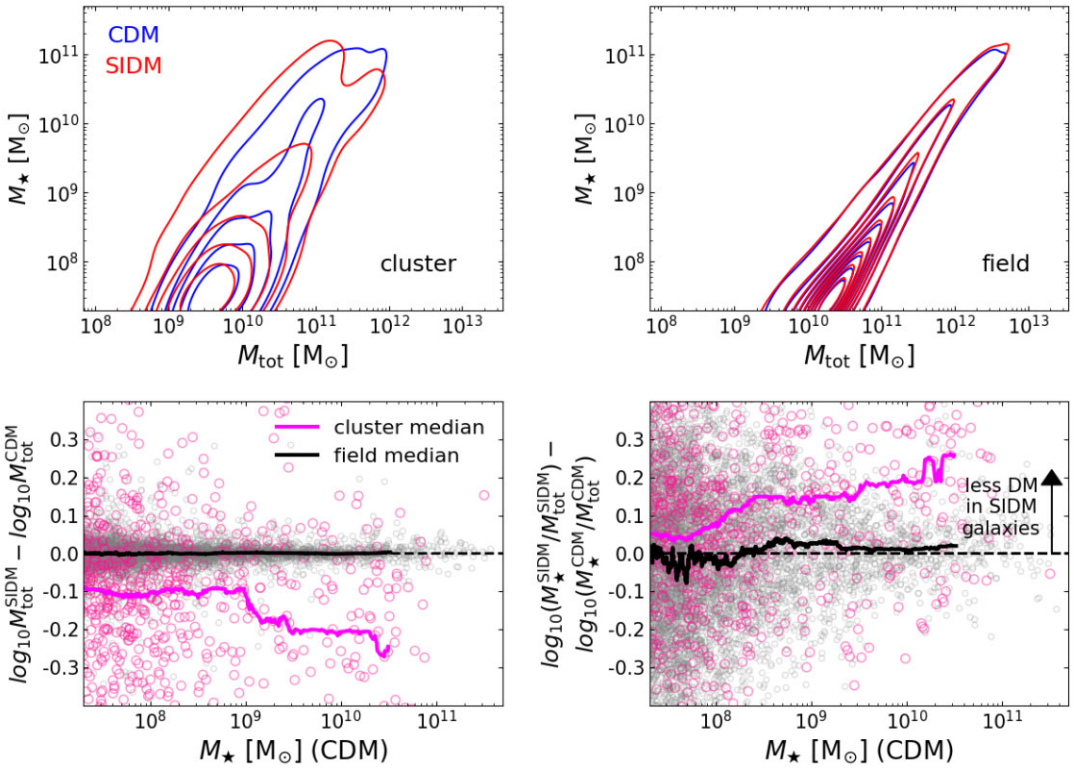

Figure 4. SHMR for galaxy pairs with >10 star particles ($M_\star \gtrsim 5 \times 10^7$ M$_\odot$), matched between CDM and SIDM simulations. Top panels: number-density contours of the stellar mass *versus* total mass in cluster CE-12 (left-hand panel) and the field (right-hand panel). Both are smoothed with the same circular Gaussian kernel of width $\sigma = 0.35$ dex: The increased scatter inside a cluster is real. A version for all (including unmatched) galaxies looks qualitatively similar. Bottom panels: the difference in total mass (left-hand panel) and stellar-to-halo mass (right-hand panel) between the SIDM and CDM galaxy populations. Pink points show matched galaxy pairs in cluster CE-12, with the running median overlaid; grey points show pairs in the field. The effect of SIDM is greatest for more massive galaxies.

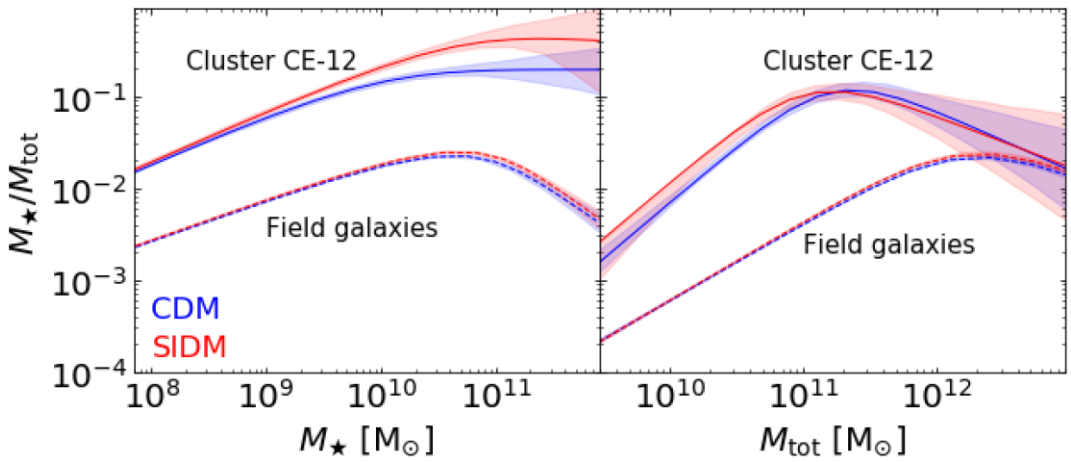

Figure 5. Fits to the SHMRs using equation (2). Left-hand panel: the SHMR as a function of stellar mass. Fits to the cluster galaxies in CE-12 are shown as solid lines and fits to field galaxies as dashed lines. Blue and red lines represent the CDM and SIDM versions of a given simulation, respectively. Shaded regions represent the 68 per cent confidence regions, obtained from the 16th and 84th percentiles of the MCMC chain. Right-hand panel: similar to the left-hand panel, but now for the SHMR as a function of halo mass. The fits to the galaxies in CE-05 are similar but noisier, because that cluster has fewer member galaxies.

(35 per cent) for the most massive cluster member galaxies. We then fit the Moster et al. (2013) relation, as described in Section 2.3. We fit all galaxies, not just those matched between simulations (as would be done with observational data). Because this adds some almost-stripped galaxies, this raises the normalization of the SHMR at low masses by a factor of ∼1.5 for both CDM and SIDM, and moves the location of the turnover within its (considerable) statistical uncertainty. The best fits are shown in Fig. 5, and the best-fitting parameters are listed in Table 3.

We find that the SHMR of SIDM field galaxies is indistinguishable from that of CDM field galaxies, within the precision possible using our limited number of simulated galaxies. This is expected since

Table 3. The best-fitting parameters of the SHMR (equation 2) for field galaxies and for cluster galaxies within $2R_{200}$ and R_{200} of CE-12. The 68 per cent confidence intervals are the difference between the 16th and 84th percentiles of the marginalized 1D posteriors.

	Fit to $M_{\rm tot}(M_\star)$		Fit to $M_\star(M_{\rm tot})$	
	CDM	SIDM	CDM	SIDM
	Field galaxies			
$\log_{10}M_1$	$12.09^{+0.06}_{-0.05}$	$12.11^{+0.06}_{-0.05}$	$12.22^{+0.05}_{-0.05}$	$12.2^{+0.05}_{-0.05}$
N	$0.022^{+0.001}_{-0.001}$	$0.024^{+0.001}_{-0.001}$	$0.021^{+0.002}_{-0.001}$	$0.023^{+0.002}_{-0.001}$
β	$0.81^{+0.02}_{-0.02}$	$0.81^{+0.02}_{-0.02}$	$0.84^{+0.02}_{-0.02}$	$0.86^{+0.02}_{-0.02}$
γ	$0.46^{+0.04}_{-0.04}$	$0.48^{+0.04}_{-0.04}$	$0.6^{+0.07}_{-0.07}$	$0.57^{+0.07}_{-0.07}$
$\sigma_{\rm M}$	$0.215^{+0.002}_{-0.002}$	$0.214^{+0.002}_{-0.002}$	$0.278^{+0.003}_{-0.003}$	$0.281^{+0.003}_{-0.003}$
	Cluster galaxies ($R < 2R_{200}$)			
$\log_{10}M_1$	$10.55^{+0.29}_{-0.24}$	$10.84^{+0.47}_{-0.35}$	$11.23^{+0.2}_{-0.24}$	$11.02^{+0.25}_{-0.23}$
N	$0.1^{+0.02}_{-0.03}$	$0.26^{+0.37}_{-0.11}$	$0.11^{+0.02}_{-0.02}$	$0.26^{+0.29}_{-0.03}$
β	$1.27^{+0.13}_{-0.17}$	$1.27^{+0.13}_{-0.22}$	$1.23^{+0.15}_{-0.18}$	$1.27^{+0.15}_{-0.18}$
γ	$0.0^{+0.19}_{-0.19}$	$0.08^{+0.42}_{-0.43}$	$0.66^{+0.34}_{-0.39}$	$0.08^{+0.37}_{-0.4}$
$\sigma_{\rm M}$	$0.36^{+0.01}_{-0.01}$	$0.41^{+0.01}_{-0.01}$	$0.62^{+0.02}_{-0.02}$	$0.41^{+0.03}_{-0.03}$
	Cluster galaxies ($R < R_{200}$)			
$\log_{10}M_1$	$10.53^{+0.29}_{-0.25}$	$10.85^{+0.3}_{-0.2}$	$11.25^{+0.29}_{-0.25}$	$11.01^{+0.43}_{-0.43}$
N	$0.14^{+0.04}_{-0.04}$	$0.5^{+0.34}_{-0.14}$	$0.16^{+0.04}_{-0.05}$	$0.5^{+0.92}_{-0.09}$
β	$1.28^{+0.14}_{-0.18}$	$1.37^{+0.12}_{-0.17}$	$1.19^{+0.2}_{-0.24}$	$1.37^{+0.35}_{-0.55}$
γ	$0.06^{+0.21}_{-0.2}$	$0.41^{+0.38}_{-0.26}$	$0.6^{+0.44}_{-0.51}$	$0.41^{+0.53}_{-0.63}$
$\sigma_{\rm M}$	$0.34^{+0.01}_{-0.01}$	$0.39^{+0.01}_{-0.01}$	$0.62^{+0.03}_{-0.03}$	$0.39^{+0.04}_{-0.04}$

field galaxies are dominated by stars, and very inefficiently affected by SIDM interactions. The SHMR for SIDM cluster galaxies is also well fitted using the functional form of Moster et al. (2013), but with different best-fitting parameters to the CDM cluster galaxies.

The SHMRs for CDM and SIDM cluster galaxies are distinguishable at the high-mass end, when binning by stellar mass. Fortunately, it is possible to measure this observationally. We find that cluster galaxies within $2R_{200}$ with stellar mass 10^{10}–10^{11} $\rm M_\odot$ have $M_\star/M_{\rm tot}$ 8 times higher than field galaxies in a CDM universe, but 13 times higher in an SIDM universe, or in other words, the SHMR of the SIDM galaxies is $\log_{10}(13/8) \sim 0.21$ dex above the SHMR of the CDM galaxies. For cluster galaxies within R_{200}, we find that these numbers increase to 10 and 20 (the best-fitting parameters are included in Table 3, but the fits are not shown in Fig. 5). There is considerable scatter, $\sigma_{\rm M} \sim 0.4$ dex, in the SMHRs at these masses. To distinguish the SHMRs at 3σ, the scatter needs to be less than $0.21/3 = 0.07$ dex. From $0.4/\sqrt{N} < 0.07$, we find that it would require noise-free measurements, e.g. from galaxy–galaxy strong lensing, of ∼32 cluster galaxies to distinguish between these values at 3σ, assuming that the SHMR for field galaxies is well known. It would be more challenging to measure other quantities like the slope of the SHMR at low masses, or the position of the turnover, because these vary by less than 5 per cent with different DM.

4.2 The stripping factor

Another measure used to express the mass lost from cluster galaxies is the 'stripping factor' (Niemiec et al. 2019)

$$\tau_{\rm strip}(M_\star) \equiv 1 - \frac{\widetilde{M}_{\rm tot,cluster}(M_\star)}{\widetilde{M}_{\rm tot,field}(M_\star)}, \quad (5)$$

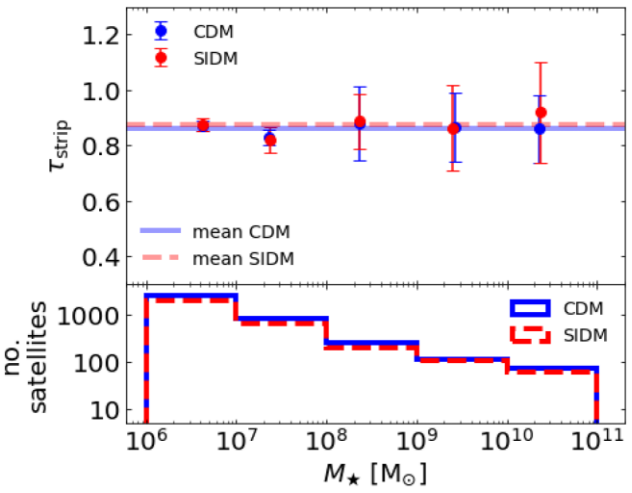

Figure 6. Top panel: $\tau_{\rm strip}$ (equation 5) as a function of mean stellar mass in five stellar bins. The results for the galaxies in the CDM and SIDM versions of CE-12 are plotted in blue and red, respectively. The horizontal solid blue and dashed red line are the mean $\tau_{\rm strip}$ of the CDM and SIDM galaxies, respectively. The mean stripping factor has a value of 0.86 ± 0.03 and 0.87 ± 0.04 for the CDM and SIDM satellites, respectively. The results for cluster CE-05 are 0.83 ± 0.04 and 0.85 ± 0.04. Bottom panel: histogram of number of galaxies in the same five stellar bins as plotted in the top panel. Again blue represents CDM and red SIDM.

where $\widetilde{M}_{\rm tot,cluster}(M_\star)$ and $\widetilde{M}_{\rm tot,field}(M_\star)$ are the median total mass of cluster and field galaxies in a bin of stellar mass $M_\star$. This definition is motivated by a model in which a galaxy's star formation is quenched as it enters a cluster. Since no new stars are formed, field galaxies of a given stellar mass act as the progenitors of cluster galaxies with the same stellar mass.

We split our sample of cluster (CE-12) and field galaxies into logarithmic bins of 1 dex in stellar mass ranging from 10^6 to 10^{11} $\rm M_\odot$, and calculate the stripping factor in each bin; the result is shown in Fig. 6. The errors on the stripping factors are calculated using bootstrapping.

The difference between CDM and SIDM is not significant in this measure, although the largest hint of a difference again appears to be in galaxies with high stellar mass. The mean stripping factor of galaxies inside $2R_{200}$ at $z = 0$ is 0.86 ± 0.03 and 0.87 ± 0.04 for the CDM and SIDM version of cluster CE-12, respectively (blue solid and red dashed horizontal lines in Fig. 6), and there is little scatter about this value in the different stellar mass bins. For massive galaxies with $10^{10} < M_\star < 10^{11}$ $\rm M_\odot$, the mean stripping factor for SIDM is $\mathcal{O}(10^{-2})$ higher than for CDM, but this is much smaller than statistical uncertainty. More stripping occurs in the inner parts of the cluster, and the stripping factors rise to 0.88 ± 0.03 and 0.90 ± 0.05 for galaxies inside R_{200}. Again there is little hope for observational discrimination.

Stripping factors are reduced in the lower mass cluster CE-05, to 0.83 ± 0.04 and 0.85 ± 0.04 for the CDM and SIDM versions of galaxies within $2R_{200}$ with again little scatter about these values. A more massive cluster seems to increase slightly both the stripping of mass and the effect of self-interactions.

4.3 The number and radial distribution of cluster galaxies

There are ∼20 per cent fewer member galaxies in the SIDM version of a given cluster at $z = 0$ (Table 1). Most of the discrepancy is in

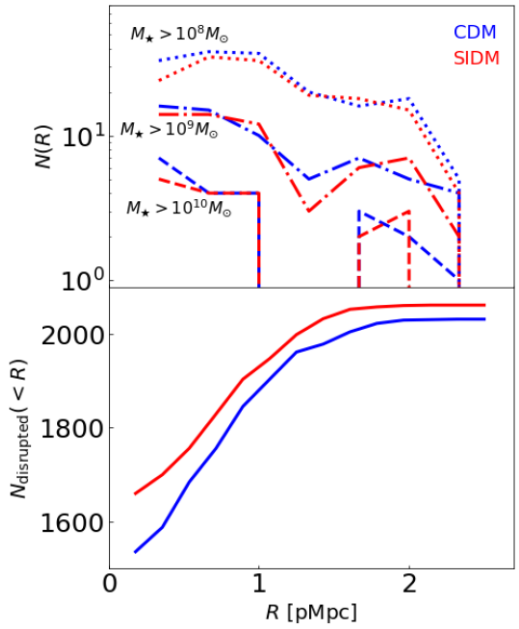

Figure 7. Top panel: the radial distribution of galaxies that survive until $z = 0$, in CDM and SIDM versions of cluster CE-05. The only useful difference is the slight reduction of SIDM galaxies inside the cluster core. Bottom panel: the last known location of galaxies that did not survive until $z = 0$. Cumulative number of galaxies inside a given radius, in the simulation snapshot immediately before they were disrupted.

the central ∼100 kpc, which is also where the most disruption takes place of SIDM galaxies whose CDM counterparts survive (Fig. 7). This is consistent with our earlier findings that SIDM barely changes the orbits of galaxies, but makes them more susceptible to disruption (Section 3.2). Cluster outskirts contain similar numbers of galaxies, with the populations continually replenished by objects infalling from the field.

It would be difficult to distinguish between CDM and SIDM using cluster richness, given the intrinsic scatter in the mass–richness relation (Simet et al. 2017; Murata et al. 2019; Hilton et al. 2021). It is probably also difficult to distinguish between CDM and SIDM using the radial distribution of cluster galaxies. We find that 33 per cent and 36 per cent of galaxies reside inside $0.5R_{200}$ in the CDM version of clusters CE-05 and CE-12, compared to 30 per cent and 26 per cent in the SIDM versions. More simulations are needed to determine the population mean and intrinsic scatter, but the difference is likely to be washed out by projection effects (of outlying members in front of/behind the cluster core, and field galaxies on to cluster outskirts).

5 DISCUSSION AND CONCLUSIONS

We studied the effects of self-interactions on the mass stripping of galaxies as they fall into galaxy clusters by comparing cosmological simulations with and without DM self-interactions. When a galaxy falls into a cluster, DM interactions accelerate the rate of mass stripping. Over 33 per cent of galaxies in an SIDM cluster can be entirely disrupted by the present time, compared to 20 per cent in a CDM cluster. Unfortunately, the disrupted galaxies (which are the most different between CDM and SIDM) are no longer observable. The orbits of surviving galaxies are essentially unchanged, and disrupted galaxies are continually replaced by new ones falling into the cluster. When comparing matched galaxies between the CDM and SIDM versions of a given cluster (Section 3), we find significant differences in mass-loss. However, when we only look at the population of galaxies remaining in the cluster at $z = 0$ (Section 4), we find considerably smaller differences. SIDM galaxies are more susceptible to disruption, so there is a large group of disrupted SIDM galaxies that does not contribute to the signal at $z = 0$.

Potentially observable ways to discriminate between CDM and SIDM include the (high mass normalization of the) SHMR of galaxies in clusters, compared to galaxies in the field, or the stripping factor, both of which describe the mass of the DM in a galaxy of fixed stellar mass. We found a 25 per cent increase in the ratio of stellar-to-total mass of SIDM galaxies with stellar mass $M_\star > 5 \times 10^7\,{\rm M}_\odot$. The absolute normalization of the relation is likely to be needed to discriminate SIDM from CDM, but this depends to some extent on the subgrid physics of the simulations. However, as in the field, the relation is nearly indistinguishable for a CDM and SIDM universe, one could use the difference between the field and cluster relations at a given stellar mass to try and discriminate between the two models. From the left-hand panel of Fig. 5, we find that, at approximately the stellar mass of the Milky Way, $10^{10.5}\,{\rm M}_\odot$, the ratio $M_\star/M_{\rm tot}$ is 8 and 13 times higher in the cluster compared to the field for the CDM and SIDM versions of CE-12, respectively.

Previous DM-only simulations (Bhattacharyya et al. 2021) predicted larger differences between SIDM and CDM, probably because of the way stars were assigned to galaxies after the simulation using a semi-analytic model. In DM-only SIDM simulations, subhaloes form cores more easily than when baryons are included, making them more easily disrupted. In contrast, our simulations co-evolved a population of baryons and SIDM. In the full hydrodynamical simulation, a large number of cluster galaxies fail to form cores or have their cores re-contracted by baryons, and so they are more durable.

We simulated a velocity-independent SIDM cross-section. As all galaxies orbit at a velocity approximately equal to the velocity dispersion of the cluster, they would experience the same effective cross-section even if a velocity dependence was introduced. However, the scattering rate of DM–DM interactions in the galaxy itself would be different for subhaloes of different masses. As internal scattering can change the structure of galaxy haloes, tidal stripping could act differently at different masses. To test the effects on the SHMR, simulations would need to be run with a velocity dependence.

In the future, it would be informative to simulate more SIDM clusters (with and without velocity dependence). While the C-EAGLE suite comprises 30 simulated CDM clusters, only two have been re-run with SIDM. It is also important to note that a cross-section of $\sigma/m = 1{\rm cm}^2\,{\rm g}^{-1}$ has arguably already been ruled out at the $\mathcal{O}(1000\,{\rm km\,s}^{-1})$ collision velocities between particles typical in clusters. Performing the same tests with simulations for a lower cross-section would presumably produce smaller differences and would require even higher signal-to-noise observations. Future surveys, such as the *Euclid* (Laureijs et al. 2011), Rubin Legacy Survey of Space and Time (LSST; LSST Science Collaboration et al. 2009), SuperBIT (Romualdez et al. 2018), and *JWST* Cosmos-Webb survey (Casey & Kartaltepe, private communication) will provide data with higher signal-to-noise than ever before, potentially making such tests possible.

ACKNOWLEDGEMENTS

We thank Anna Niemiec for discussing the physics of infall, and Yannick Bahé and David Barnes for making the C-EAGLE data

available. We also thank the referee for the useful comments and helpful suggestions.

ES and RM are supported by the Royal Society. AR is supported by the European Research Council's Horizon2020 project 'EWC' (award AMD-776247-6). KAO and CSF acknowledge support by the European Research Council (ERC) through Advanced Investigator grant to CSF, DMIDAS (GA 786910). This work used the DiRAC@Durham facility managed by the Institute for Computational Cosmology on behalf of the STFC DiRAC HPC Facility (www.dirac.ac.uk). The equipment was funded by BEIS capital funding via STFC capital grants ST/K00042X/1, ST/P002293/1, ST/R002371/1, and ST/S002502/1, Durham University and STFC operations grant ST/R000832/1. DiRAC is part of the National e-Infrastructure.

DATA AVAILABILITY

The CDM simulations were introduced by Bahé et al. (2017) and the SIDM simulations by Robertson et al. (2018). Data from those works are available from the original papers.

REFERENCES

Bahé Y. M. et al., 2017, MNRAS, 470, 4186
Barnes D. J. et al., 2017, MNRAS, 471, 1088
Bhattacharyya S., Adhikari S., Banerjee A., More S., Kumar A., Nadler E. O., Chatterjee S., 2021, preprint (arXiv:2106.08292)
Binney J., Tremaine S., 2008, Galactic Dynamics, 2nd edn. Princeton Univ. Press, Princeton
Bradač M., Allen S. W., Treu T., Ebeling H., Massey R., Morris R. G., von der Linden A., Applegate D., 2008, ApJ, 687, 959
Bullock J. S., Boylan-Kolchin M., 2017, ARA&A, 55, 343
Burkert A., 2000, ApJ, 534, L143
Clowe D., Bradač M., Gonzalez A. H., Markevitch M., Randall S. W., Jones C., Zaritsky D., 2006, ApJ, 648, L109
Crain R. A. et al., 2015, MNRAS, 450, 1937
Davis M., Efstathiou G., Frenk C. S., White S. D. M., 1985, ApJ, 292, 371
Dawson W. A. et al., 2012, ApJ, 747, L42
Di Cintio A., Tremmel M., Governato F., Pontzen A., Zavala J., Bastidas Fry A., Brooks A., Vogelsberger M., 2017, MNRAS, 469, 2845
Dolag K., Borgani S., Murante G., Springel V., 2009, MNRAS, 399, 497
Dooley G. A., Peter A. H. G., Vogelsberger M., Zavala J., Frebel A., 2016, MNRAS, 461, 710
Foreman-Mackey D., Hogg D. W., Lang D., Goodman J., 2013, PASP, 125, 306
Frenk C. S., White S. D. M., 2012, Ann. Phys., 524, 507
Harvey D., Massey R., Kitching T., Taylor A., Tittley E., 2015, Science, 347, 1462
Hilton M. et al., 2021, ApJS, 253, 3
Jiang L., Helly J. C., Cole S., Frenk C. S., 2014, MNRAS, 440, 2115
Laureijs R. et al., 2011, Euclid Definition Study Report. preprint (arXiv:1110.3193)
LSST Science Collaborations and LSST Project, 2009, LSST Science Book, Version 2.0 (arXiv:0912.0201)
McCarthy I. G., Frenk C. S., Font A. S., Lacey C. G., Bower R. G., Mitchell N. L., Balogh M. L., Theuns T., 2008, MNRAS, 383, 593
Massey R., Kitching T., Richard J., 2010, Rep. Prog. Phys., 73, 086901
Meneghetti M., Yoshida N., Bartelmann M., Moscardini L., Springel V., Tormen G., White S. D. M., 2001, MNRAS, 325, 435
Moster B. P., Naab T., White S. D. M., 2013, MNRAS, 428, 3121
Murata R. et al., 2019, PASJ, 71, 107
Niemiec A., Jullo E., Giocoli C., Limousin M., Jauzac M., 2019, MNRAS, 487, 653
Oman K. A., Bahé Y. M., Healy J., Hess K. M., Hudson M. J., Verheijen M. A. W., 2021, MNRAS, 501, 5073
Peter A. H. G., Rocha M., Bullock J. S., Kaplinghat M., 2013, MNRAS, 430, 105
Planck Collaboration XVI et al., 2014, A&A, 571, A16
Planck Collaboration XIII et al., 2016, A&A, 594, A13
Robertson A., Massey R., Eke V., 2017a, MNRAS, 465, 569
Robertson A., Massey R., Eke V., 2017b, MNRAS, 467, 4719
Robertson A. et al., 2018, MNRAS, 476, L20
Robertson A., Harvey D., Massey R., Eke V., McCarthy I. G., Jauzac M., Li B., Schaye J., 2019, MNRAS, 488, 3646
Rocha M., Peter A. H. G., Bullock J. S., Kaplinghat M., Garrison-Kimmel S., Oñ;orbe J., Moustakas L. A., 2013, MNRAS, 430, 81
Romualdez L. J. et al., 2018, in Evans C. J., Simard L., Takami H., eds, Proc. SPIE Conf. Ser., Vol. 10702, Ground-Based and Airborne Instrumentation for Astronomy VII. SPIE, Bellingham, p. 107020R
Schaye J. et al., 2015, MNRAS, 446, 521
Simet M., McClintock T., Mandelbaum R., Rozo E., Rykoff E., Sheldon E., Wechsler R. H., 2017, MNRAS, 466, 3103
Spergel D. N., Steinhardt P. J., 2000, Phys. Rev. Lett., 84, 3760
Springel V., White S. D. M., Tormen G., Kauffmann G., 2001, MNRAS, 328, 726
Tulin S., Yu H.-B., 2018, Phys. Rep., 730, 1
van den Bosch F. C., Aquino D., Yang X., Mo H. J., Pasquali A., McIntosh D. H., Weinmann S. M., Kang X., 2008, MNRAS, 387, 79
Vega-Ferrero J., Dana J. M., Diego J. M., Yepes G., Cui W., Meneghetti M., 2021, MNRAS, 500, 247
Wittman D., Golovich N., Dawson W. A., 2018, ApJ, 869, 104

This paper has been typeset from a TEX/LATEX file prepared by the author.